Mon. Not. R. astr. Soc. (1986) **221,** 213–232

Bi-symmetric instabilities of the Kuz'min/Toomre disc

E. Athanassoula *Observatoire de Marseille, 2 Place le Verrier, 13248 Marseille Cedex 04, France*

J. A. Sellwood* *Institute of Astronomy, Madingley Road, Cambridge CB3 0HA and Kapteyn Laboratory, Postbus 800, 9700AV Groningen, The Netherlands*

Accepted 1986 February 12. Received 1986 January 24; in original form 1985 November 18

Summary. This paper reports a numerical study of the effect of random motion on the unstable bar-forming modes of one type of stellar disc mass model. From measurements of the growth rates of the few most unstable bi-symmetric modes we evaluate the stabilizing influence of both random motion and halo mass. We find that the growth rate of bars is a simple function of these two variables. Our results suggest that the large degree of random motion recently observed near the centres of galactic discs substantially reduces the halo mass needed to understand their stability.

1 Introduction

The bar instability of stellar discs has proved a major obstacle to our understanding of disc-galaxy dynamics; before we can comprehend spiral structure, we must construct plausible stable (or nearly stable) equilibrium models. This first step has proved much more difficult than expected, since all studies of self-gravitating discs of stars supported mainly by rotation find rapidly growing global instabilities (see e.g. Toomre 1977 and Athanassoula 1984 for reviews). We begin with a discussion of current ideas which attempt to account for the apparent absence of such gross instabilities in the majority of disc galaxies and we then justify a fresh approach.

1.1 MASSIVE HALOES

The most popular idea has been that massive haloes suppress the instability. Most of the mass of dark extended haloes currently thought to surround galaxies is irrelevant, since to be any use at all the spherically distributed matter must lie *interior* to the unstable region of the disc. Ostriker & Peebles (1973) suggested that the spheroid and inner halo should contain between 1 and 2.5× the total mass of the disc to prevent bar formation, and went on to argue for much more massive and extended haloes exterior to this. Many numerical simulations (e.g. Hohl 1971; Hockney &

* Present address: Department of Astronomy, The University, Manchester M13 9PL.

Brownrigg 1974; James & Sellwood 1978; Sellwood 1980; Efstathiou, Lake & Negroponte 1982) have confirmed that large fractions of spherically distributed mass can prevent bar formation. The physical explanation for this was given by Toomre (1981) who showed that decreasing the disc's contribution to the rotation curve reduces the length-scales of disc instabilities to the point where they cease to be global.

Observational tests of this hypothesis are inconclusive since firm values of inner halo to disc mass ratios are very hard to obtain. The mass distribution within the Milky Way is probably the most tightly constrained of any galaxy but there is still wide disagreement over the relative quantities of disc and spherical matter in the various proposed mass models (see Schmidt 1985 for a review). Efstathiou *et al.* (1982) deduced the halo masses required, according to their criterion, to account for the absence of bars in a number of galaxies. They found that the necessary halo mass implied rather uncomfortably low mass-to-light ratios for the discs of their sample of galaxies.

In our view, a more powerful argument against stabilization by massive inner haloes comes from the observed preference for two-armed spiral patterns in galaxies. The theory of 'swing amplification' (Toomre 1981) seems to imply that haloes massive enough to prevent bars would simultaneously inhibit the development of all bi-symmetric features. Multi-armed patterns, such as developed in the simulations of Sellwood & Carlberg (1984), would be favoured. Thus we remain unconvinced that sufficient spheroidal matter is present near the centres of galaxies to alone guarantee stability.

1.2 IMPASSABLE CENTRES

Toomre (1981) proposes an alternative solution to the bar instability problem: breaking the feedback cycle which, he argues, is the origin of the instability. This can be achieved either through a high circular velocity near the centre (which forces inwardly propagating density waves to encounter an inner Lindblad resonance), or by a depression in the surface density of the disc at the centre. Sellwood (1985) has recently shown that the inner Lindblad resonance mechanism contributes to the bar stability of our Galaxy. (Ironically the halo was irrelevant to the bar stability of the disc but was required to prevent even more destructive one-armed instabilities!) Although it is likely that other galaxies having sharply rising rotation curves near the centre may avoid bar instabilities in this way, it is of no help in galaxies having gently rising rotation curves.

1.3 HOT DISCS

In this paper we examine a third possible solution – that large degrees of random motion among the disc stars can suppress the bar instability. This alternative has not hitherto been thought particularly attractive (e.g. Ostriker & Peebles 1973), since the only good determination of the extent of random motion amongst disc stars, namely for the solar neighbourhood, indicates that the dispersion of the radial velocity components is roughly one fifth of the mean orbital velocity. However, this measurement is at a point far from the axis of rotation, and dynamical considerations (local stability arguments and the observed constant scale height of external edge-on galaxies) require that the ratio of rotational to pressure support should increase markedly towards the centre.

Such an increase has recently been observed in our galaxy by Freeman (private communication) and can also be deduced from Habing *et al.*'s (1983) observations of OH/IR stars near the Galactic Centre, if they are disc population objects. These appear to have a radial velocity dispersion of some $150\,\mathrm{km\,s^{-1}}$. Moreover, observations (e.g. Kormendy 1981, 1984;

Bosma & Freeman (unpublished); Illingworth & Schechter 1982, van der Kruit & Freeman 1985; Kormendy & Illingworth 1985, in preparation) of the velocity dispersions in nearby galaxies have reported values almost as large as the mean orbital motion in the inner part of the disc.

This degree of random motion must have a considerable stabilizing influence, but just how substantial is not known. Full global stability analyses of stellar discs with velocity dispersion are difficult (Kalnajs 1977) and have so far been accomplished in only a few special cases. All three existing studies – Kalnajs (1972, 1978) and Zang (1976, see also Toomre 1977) – have found, not surprisingly, that the growth rate of unstable modes decreases with increasing random motion amongst the disc stars. However, the only two known stable stellar discs, which were constructed by Kalnajs (1972), rotate uniformly. All the self-gravitating, differentially rotating discs studied by Kalnajs (1978) and Zang (1976) exhibit some, perhaps slowly growing, global instabilities.

Global modes in gaseous discs are somewhat easier to calculate and several such studies have been reported. In particular, Bardeen (1975) and Aoki, Noguchi & Iye (1979) showed that bi-symmetric modes could probably be stabilized by increasing pressure support before the net rotation rate became insignificant. However, the similarities between the behaviour of stellar discs and gaseous polytropes decrease as pressure support rises.

Large N-body codes have also been used to study instabilities in stellar discs, but surprisingly few experiments having high degrees of pressure support have been reported. A notable exception was described by Hohl (1971), who constructed an apparently stable axisymmetric model from the final barred state of a previous simulation. He achieved this by reshuffling all stars in the model by random shifts in azimuth in such a way that the bar was removed. Although the model was probably not in perfect equilibrium after this procedure, Hohl noted that little change occurred during the subsequent evolution, which he followed for six rotation periods.

In this paper we describe a quantitative determination of the stabilizing effect of random motion for only one mass distribution. Our results, therefore, do not permit us to draw general conclusions for arbitrary mass distributions but we hope that thorough studies of several specific cases will ultimately achieve this end.

Our main results are described in Sections 5 and 6 and are summarized in Fig. 2. In Section 2 we introduce the mass model and distribution functions chosen for this study. Section 3 gives a few technical details of our numerical parameters, and we justify our neglect of thickness corrections in Section 4. We interpret our results in the light of current theoretical work on the unstable modes of stellar discs in Section 7 and consider the implications of the recent observations in Section 8. Our numerical techniques have been described previously (Sellwood & Athanassoula 1986, hereafter Paper I).

2 Initial conditions

2.1 MASS DISTRIBUTION

All the models described in this paper have the surface density distribution, Σ, of a flat Kuz'min disc (model 1 of the sequence proposed by Toomre 1963)

$$\Sigma(r)=\frac{Mq}{2\pi b^2}\left(1+\frac{r^2}{b^2}\right)^{-3/2}, \tag{1}$$

where q is the fraction of the total mass, M, represented by the disc stars and b is a length scale. The gravitational potential in the plane of this disc has the same form as that of a Plummer sphere, so when $q<1$, the remaining mass can be thought of as residing in a spherically symmetric halo

component having that volume density distribution, namely

$$\varrho(r)=\frac{3M(1-q)}{4\pi b^3}\left(1+\frac{r^2}{b^2}\right)^{-5/2},$$

with the same length scale as the disc.

As the fraction of the radial force in the plane due to the disc is also equal to q, all equilibrium distribution functions for the pure disc need only to be rescaled by q to be used as equilibrium functions for arbitrary q. The circular velocity curve in our models (dashed curve in Fig. 1) has a maximum at a radius of $r_{\rm m}=\sqrt{2b}$,

We limit the radial extent of the infinite disc (equation 1) in two ways: first we discard all stars having sufficient energy to reach radii greater than $6b$, then, in order to avoid too abrupt a discontinuity, we taper the edge in angular momentum from $r=5b$ to $r=6b$.

2.2 AXISYMMETRIC STABILITY

Toomre (1964) showed that the local axisymmetric stability of a stellar disc is governed by the parameter Q:

$$Q=\frac{\sigma_u\varkappa}{3.36G\Sigma}, \tag{2}$$

where σ_u is the dispersion of the radial velocity components of the disc stars (assumed small and Gaussian) and $\varkappa$ is the usual epicyclic frequency. When Q exceeds one, local axisymmetric stability is ensured.

Since the surface density enters in the denominator, the Q in a model with $q<1$ is simply higher everywhere, by the factor q^{-1}, than in the full-mass disc having the same form of distribution function.

2.3 DISTRIBUTION FUNCTIONS

Our principal reason for selecting the Kuz'min/Toomre disc was that it is relatively easy to devise distribution functions for its simple potential well. Two families were already available in the literature, and were able to devise another when neither offered the Q profiles we sought.

2.3.1 Miyamoto functions

Miyamoto (1971) proposed a set of distribution functions for this disc in which the mean orbital velocity of the stars is a fixed fraction of the circular velocity. They are characterized by a free parameter, $m_{\rm M}$, which determines this fraction, and therefore the degree of pressure support. In Fig. 1(a)–(c) we plot the radial run of $\langle v\rangle$, σ_u and Q for the $m_{\rm M}=5$ function for $q=1$, taking into account our form for truncation of the disc at $r=6b$. Although σ_u decreases with radius, Q increases outwards.

A small proportion of retrograde stars, having orbital speeds almost equally large as the direct stars, are required to keep the distribution function positive everywhere. We used the minimum fraction of retrograde stars to construct the initial velocities for our simulation.

2.3.2 Kalnajs functions

Kalnajs (1976) proposed an alternative family for the same disc, again characterized by a free parameter, $m_{\rm K}$, which determines the degree of non-circular motion. When $m_{\rm K}=3$, the

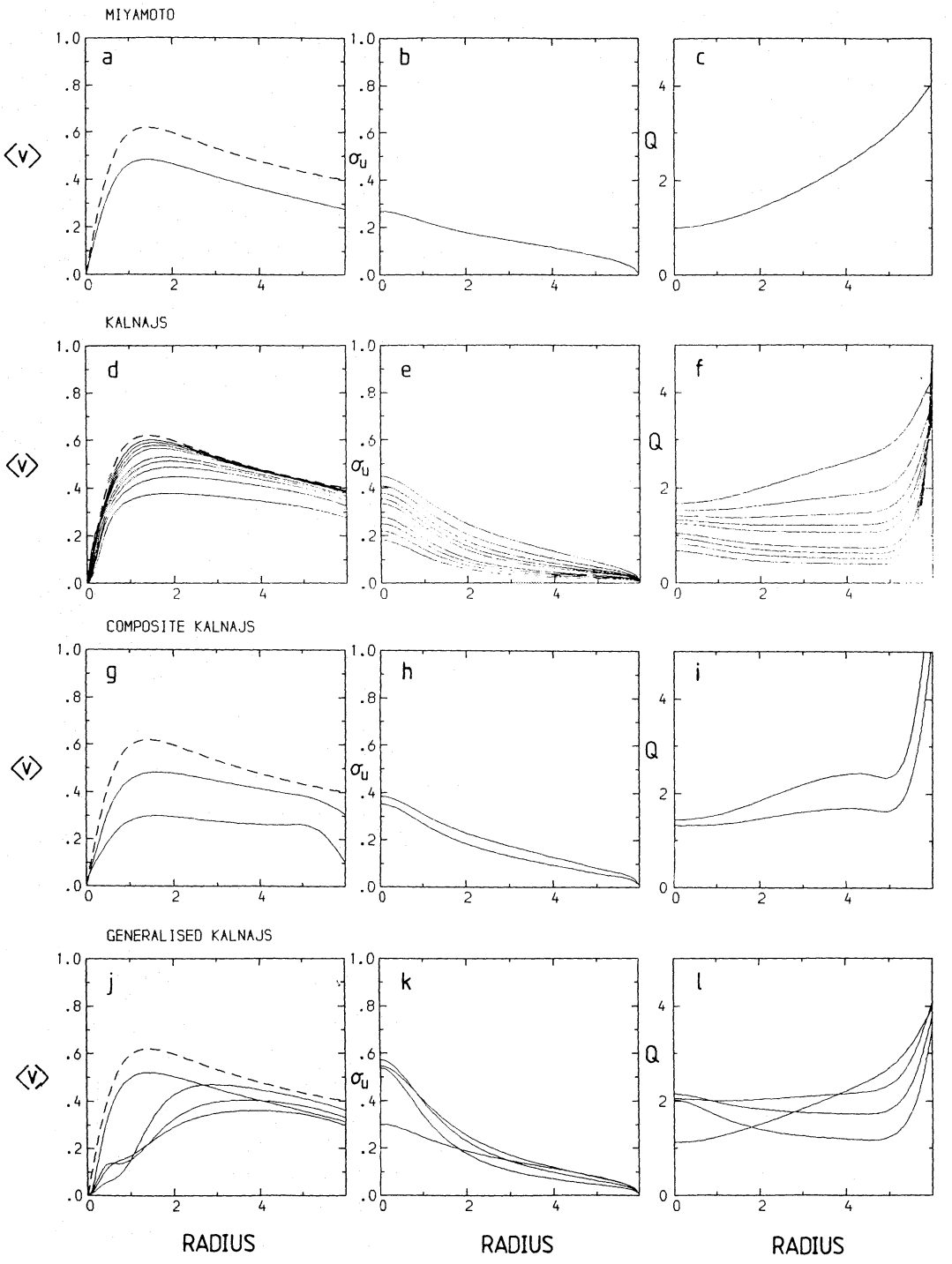

Figure 1. Radial variations of $\langle v \rangle$. σ_u and Q for all distribution functions of the Kuz'min/Toomre disc used in this paper. The dashed curve shows the circular velocity for this potential. All other curves are computed from the actual distribution functions used, taking into account our adopted taper of the disc at the outer edge, and the fractions of retrograde stars used. (a)–(c) A Miyamoto (1971) type function with $m_M=5$. (d)–(f) Kalnajs (1976) type functions with $m_K=4, 5, 6, 7, 8, 12, 15, 20$ and 30. (g)–(i) Composite Kalnajs functions made up of $m_K=20$ and an $m_K=3$ or 4 function. (j)–(l) Generalized Kalnajs (see Appendix A) functions with $(m_L, \beta)=(5,2), (6,3), (8,4)$ and $(3.5, -4)$. In all cases, the lowest value for m gives the highest Q at large radii. Q values for models with $q<1$ should be rescaled by the factor q^{-1}.

distribution function is independent of angular momentum, and the disc is completely pressure supported. As m_K rises, rotational support increases and as $m_K \to \infty$, the orbits of all stars become circular. The radial velocities of the stars have a distribution close to Gaussian, as do the tangential components away from the centre.

Fig. 1(d)–(f), show the mean tangential speed, velocity dispersion and Q profiles for those members of this family used here, again for $q=1$ and taking into account our tapering towards the edge (which causes the steep rise in Q at the outer edge). While the cooler models have a nearly constant value over most of the disc, Q also rises outwards in the hotter models of this family.

Since these functions depend upon only even powers of the angular momentum, J, any arbitrary fraction of stars can have retrograde orbits. In our simulations, we introduce retrograde stars near the centre only, according to the prescription given in Paper I, in order to make the distribution of tangential velocities smooth across zero, as shown in Fig. 1(d).

2.3.3 *Composite functions*

More distribution functions can be constructed by superposition of two or more equilibrium functions, thereby generating multiple 'populations' within the disc. We have experimented with just two such models. In each, 50 per cent of the mass was in a cool ($m_K=20$) population and the other 50 per cent in a hot ($m_K=3$ or 4) population.

The total distributions of stellar radial velocities in our two composite models, therefore, have both broad and narrow components. In Fig. 1(g)–(i) we show the same properties as before, defined by calculating the first or second moments of this combined distribution function. Each population had a separate fraction of retrograde stars according to the value of J_c which we adopt for that function in the single population models. For the $m_K=3$ component, we set $J_c=\infty$, causing equal numbers of stars to orbit in each direction and the population to have no net rotation.

Clearly it is possible to construct models having an infinity of populations by combining suitably weighted fractions of an entire set of functions, but we have not done so.

2.3.4 *Generalized Kalnajs functions*

Neither of the published families of distribution functions offers models with declining Q profiles, or even hot discs with constant Q. We wished to experiment with hot models having flat or declining Q profiles, since this seemed to us to be the likely situation in real galaxies.

It proved surprisingly difficult to achieve such an apparently simple objective. A shallow potential well is unable to confine stars with large energies of non-circular motion to the central part of the disc. For declining Q profiles, σ_u must decrease more rapidly than $\Sigma/\varkappa$, but, in our chosen mass distribution, this combination decreases faster than the square root of the potential!

However, we were able to devise a distribution function giving a Q profile peaked towards the middle, which we describe more fully in Appendix A. These functions have two free parameters, m_L and β. When β is zero they reduce to a Kalnajs function with $m_L=m_K$, whereas when it is positive or negative the centre is respectively hotter or cooler than the equivalent Kalnajs function. We plot the same properties for the members of this family used in our simulations in Fig. 1(j)–(l).

An unpleasant feature of these functions when $\beta>0$ is that f does not decrease monotonically with energy at fixed angular momentum. As a result, the radial velocity profiles are double peaked, which is why the second moment can be higher without introducing unbound stars. Again we have naïvely taken the second moment of the radial velocity distribution to define Q in equation (2) even where the distribution is non-Gaussian. Contours of this function are given for one model in Fig. 7.

3 Computational implementation

We represent the disc component by 40 000 particles chosen from these distribution functions according to the procedure described in Paper I. They are grouped in 10s but otherwise smoothly distributed in energy and angular momentum.

The particles are constrained to move in a plane and their mutual gravitational forces are derived from the usual softened potential, with the softening length being $0.2b$. The polar grid used for the force determination has 70×96 points and forces are further smoothed by discarding all azimuthal Fourier harmonics higher than nine. By spacing 10 stars almost evenly around a ring, we contrive that tangential forces are very small at the start.

Both disc truncation and gravity softening alter the central attraction of the active disc. We compensate for these effects by adding a correcting force throughout the simulation that is the difference between the theoretical and computed central attraction at the start.

Our time-step was $0.08(b^3/GM)^{1/2}$ and the grid length unit was set equal to $0.1b$. However, we use units such that $G=M=b=1$ for all quantities specified in this paper.

Further details of the numerical method are given in Paper I and references therein.

4 Validity of the plane approximation

In common with most theoretical work on stellar discs, both analytic and numerical, we neglect motions normal to the plane. This simplifying approximation is likely to be valid only where the thickness of the disc is small, and we therefore require that the disc remains reasonably thin even when hot.

It seems reasonable to assume that the velocity dispersion normal to the plane, σ_w, might be half that of the radial component in the plane. This is ample to avoid 'fire hose' instabilities (Toomre 1983) and in accordance with the observed state in the solar neighbourhood. Using this condition, and the standard formula for the local z scale of an isothermal sheet ($z_0=\sigma_w^2/\pi G\Sigma$) we find that z_0 rarely exceeds $0.2b$, or less than 5 per cent of the disc outer radius, for even our hottest models.

The gravitational softening which we introduce in our models can be interpreted physically in two equivalent ways: either the gravitational field of the particles is that in a plane offset a distance, d, from the galactic plane, or each of our particles has a finite extent – they are in fact Plummer spheres with a scale size of our softening length. Either interpretation implies that much of the thickness correction which could be required for our hot disc models is quite naturally made by the use of a softening length comparable to the likely thickness.

Four groups (Hockney & Brownrigg 1974; James & Sellwood 1978; Hohl 1978; Combes & Sanders 1981) have described fully three-dimensional numerical simulations of disc galaxies but were forced, through limitations of resources (both memory and cpu time), to work with worryingly coarse grids; in particular, the thickness of their discs scarcely exceeded one grid cell. Only when the discs were made quite unreasonably thick did the evolution change at all, and then only marginally (James & Sellwood 1978). We prefer to retain the spatial resolution afforded by a two-dimensional grid and to let softening approximate the necessary correction for finite thickness.

5 Results

5.1 DESCRIPTION OF MODELS

We have run simulations of 32 models, summarized in Table 1. In columns 1, 2 and 3 we give the type of distribution function used and the values of the free parameter(s). Columns 4 and 5 give

the values of q and J_c (which determines the fraction of retrograde stars; see Paper I) and in column 6 we indicate the duration of the run. A rotation period at the 'turnover radius' (r_m) is 14.32 in these units ($G=M=b=1$).

The evolution of two of these models is illustrated in Paper I and in many respects they are typical. In the rapidly evolving cool discs with large q, the 'S' shaped feature which first appeared quickly developed into a narrow bar and a transient ring. The more random motion in the disc, the longer it took for feature to appear and the bars that formed were fatter with weaker associated spiral structure and rings. In some very hot models, no visible structure developed at all. As q decreased, the pace of the evolution was also slowed, but faint spiral features, apparently unrelated to a bar, frequently surfaced in these cool discs before the formation of the bar.

In this paper we will focus on the growth of bi-symmetric ($m=2$) disturbances in these models and we will discuss features having different symmetries in a future publication. The $m=2$ disturbances nearly always dominate; features with higher rotational symmetries are noticeable only in models with $q \leqq 0.6$, but even in these the final appearance is bar-like.

5.2 GLOBAL MODE RESULTS

We have attempted to fit a few discrete, exponentially growing modes to the Fourier spectra of all these models, during the early part of their evolution (i.e. before the appearance of visible structure in the particle distribution). The procedure we use is described in Paper I. We obtained a satisfactory fit for most runs and give our estimates of the eigenfrequencies in columns 7–12 of Table 1. The two modes with their frequencies given in parentheses may not be real, since not all our conditions for an acceptable mode were fulfilled in these two cases. Column 13 gives the quantity S, defined in Paper I, which indicates the relative magnitude of the residuals. The real part of the eigenfrequency is twice the pattern speed (for an $m=2$ disturbance) and the imaginary part is the growth rate.

The modes are arranged in Table 1 in order of decreasing pattern speed. In some cases the second or third mode grew the fastest, but in all cases in which visible features appeared, we found that it was the most rapidly rotating (*not* the most rapidly growing) mode which reached the highest amplitude in the end, and which led to a bar. We therefore designate this the 'bar mode' in the remaining discussion.

Fourier analysis of the few models with $\beta>0$ reveals a rapidly evolving bi-symmetric instability near the centre whose growth ceases abruptly before its amplitude is sufficient to cause any visible distortion of the particle distribution. These instabilities scarcely rotate at all (the eigenfrequencies during the growing phase are given in columns 11 and 12 in Table 1) and are confined to the region where the distribution of radial velocities is double peaked. We believe that they are caused by the unnatural properties of the distribution function and are unrelated to rotational instabilities. We shall discount them in the discussion sections of this paper. A fuller description of their properties is given in Appendix B.

5.3 ESTIMATED ERRORS

The reliability of these fits is reflected in the magnitude of S and in the quoted uncertainties, which indicate the total range of acceptable frequencies found during the tests described in Paper I. The number of unstable modes we were able to find was usually clear from the power spectra (see Paper I), but many more could be present in the models having cool discs and small q than we were able to identify with confidence. We give frequencies, with large uncertainties, for one or

Table 1.

Type 1	m 2	β 3	q 4	J_c 5	time 6	Re(ω_1) 7	Im(ω_1) 8	Re(ω_2) 9	Im(ω_2) 10	Re(ω_3) 11	Im(ω_3) 12	S 13
K	4	0	1.0	0.40	520	.336±.001	.020±.001					.07
K	5	0	1.0	0.30	200	.419±.002	.046±.003					.06
K	6	0	1.0	0.25	200	.465±.002	.066±.003	.330±.004	.058±.005			.05
K	6	0	0.9	0.25	240	.427±.002	.046±.003					.02
K	6	0	0.8	0.25	340	.392±.003	.036±.002	.29 ±.02	.035±.01			.23
K	6	0	0.7	0.25	480	.359±.001	.026±.002					.18
K	7	0	0.8	0.20	320	.419±.003	.041±.003	.293±.008	.055±.01			.17
K	7	0	0.7	0.20	400	.386±.005	.020±.005	.307±.005	.018±.005	.249±.003	.016±.005	.27
K	7	0	0.6	0.20	520	.355±.001	.016±.002	.278±.003	.016±.002			.25
K	8	0	1.0	0.15	160	.538±.005	.100±.002					.07
K	8	0	0.9	0.15	160	.486±.003	.067±.002	.328±.005	.055±.005			.03
K	8	0	0.8	0.15	240	.453±.001	.056±.001					.03
K	8	0	0.7	0.15	360	.425±.010	.028±.005	.365±.010	.025±.010	.269±.004	.032±.008	.22
K	8	0	0.6	0.15	400	.364±.010	.016±.010	.304±.005	.020±.010			.55
K	12	0	1.0	0.10	156	.602±.006	.112±.005	.461±.004	.098±.005			.06
K	12	0	0.9	0.10	188	.551±.010	.085±.010	.327±.010	.074±.010			.17
K	12	0	0.8	0.10	200	.510±.005	.060±.004	.420±.005	.063±.005	(.313±.004	.045±.010)	.09
K	12	0	0.7	0.10	320	.471±.002	.047±.003	.410±.010	.042±.005	.290±.010	.04 ±.01	.13
K	12	0	0.6	0.10	400	.427±.003	.027±.003	.320±.010	.035±.010	.195±.010	.035±.01	.19
K	12	0	0.5	0.10	520	.38 ±.01	.02 ±.01					.37
K	15	0	0.6	0.10	380	.45 ±.01	.04 ±.01	.32 ±.03	.07 ±.01			.34
K	20	0	0.5	0.04	532	.407±.005	.026±.010	.375±.01	.027±.015			.12
K	30	0	0.4	0.04	560	.395±.010	.017±.010					.60
C	20+3	0	1.0		320	.442±.004	.035±.001					.20
C	20+4	0	1.0		240	.500±.003	.096±.003					.05
M	5	0	1.0		128	.527±.002	.096±.001					.02
L	3.5	-4	1.0	0.20	160	.528±.005	.100±.005					.07
L	5	2	1.0	0.70	564	(.27 ±.01	.005±.005)			.045±.01	.06 ±.01	.20
L	6	3	1.0	0.60	608	.290±.003	.014±.010			.073±.005	.073±.005	.15
L	8	4	1.0	0.90	228	.345±.010	.035±.010			.02 ±.01	.075±.010	.10
L	8	4	0.9	0.90	360	.332±.003	.033±.005			.025±.001	.041±.010	.15
L	8	4	0.8	0.90	392	.323±.010	.020±.01			.023±.005	.045±.010	.28
L	8	4	0.7	0.90	220					-.003±.003	.053±.005	.30

Notes to Table 1

Col. 1. The letters indicate the type of distribution function used: K – Kalnajs, C – composite Kalnajs, M – Miyamoto and L – generalized Kalnajs.

Col. 2. The value of m_K, m_M or m_L as appropriate for the type of distribution function.

Cols 11 and 12. The values for the generalized Kalnajs models are for the different type of mode discussed in Appendix B.

two modes in these models, but these fits leave very large residuals. However, we are confident that no $m=2$ disturbance grows more rapidly in these models than the highest listed growth rate.

No analytical results for this mass distribution are available for comparison with our data. Gravity softening causes our method to systematically underestimate the growth rates that should occur in completely flat discs, but we would argue, as in Section 4, that our growth rates are probably more relevant to galaxies where hot discs would have a thickness comparable to our softening length.

6 Stability requirements

6.1 RANDOM MOTION VERSUS HALO MASS

Table 1 shows quantitatively how both halo mass and random motion slow the growth of bars, either separately, or in concert. This is illustrated in Fig. 2(a), where we plot growth rate of the *bar* mode as a function of these two parameters. As a measure of the extent of random motion we

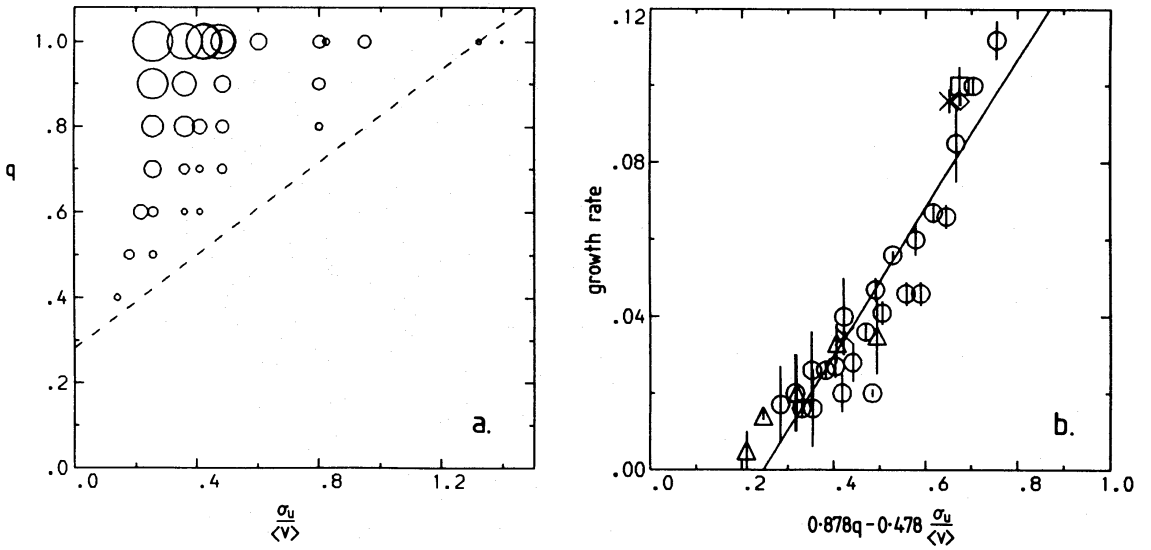

Figure 2. The growth rate of the *bar* mode as the fraction of active mass and random motion content of the disc are varied. The sizes of the circles in (a) are proportional to the growth rate in each of the models. (b) Shows the distance of each point from the best-fit plane, the error bars indicating the total range of our (internally) estimated uncertainty. The symbols denote the type of distribution function: circles – Kalnajs functions, diamond – Miyamoto function, crosses – composite Kalnajs functions, triangles – generalized Kalnajs functions +ve β and the square – generalized function with −ve β. The dashed line in (a) shows the intersection of the best fit plane with the growth rate=0 plane.

use the ratio $\sigma_u/\langle v\rangle$, evaluated at r_m. This dimensionless ratio is a directly observable quantity. (Unfortunately it is subject to considerable observational uncertainty, since it may vary quite strongly with radius. We were unable to find an alternative easily observable estimator of pressure support that did not suffer from some such defect.)

Fig. 2(a) clearly suggests that the points lie on a simple surface in this three-dimensional volume, and we have found that a plane gives a satisfactory fit. The equation of the best fit plane is

$$\text{growth rate}=0.169\,q-0.092\frac{\sigma_u}{\langle v\rangle}-0.048.$$

This fit is obtained when equal weight is given to all points, but the values of the three free parameters change very little if the points are weighted by the inverse of our estimated uncertainty. The quality of the fit to this plane can be seen in Fig. 2(b), which shows how far the points deviate from the plane. The sizes of the error bars indicate the total ranges within which we expect the growth rate to lie. There is perhaps some evidence that the surface is curved rather than planar, but we do not feel that the data justify a fit with more free parameters.

6.2 BAR-STABLE MODELS

If we accept the planar fit, we find that zero growth rates should occur along the dashed line drawn in Fig. 2(a). There are theoretical reasons to expect growth rates never to go precisely to zero (see Section 7), but several of our models close to this line failed to form any visible structure whatsoever for as long as we ran the experiments. We therefore consider this line to represent, for practical purposes, the boundary of the bar-unstable region in this mass distribution.

Thus the growth rate of the bar mode can be effectively reduced to zero by increasing the degree of random motion without the need for any halo mass at all. We can barely detect a growing disturbance in our simulation in the model with the hottest disc ($m_L=5$ and $\beta=2$). It appears to grow no faster than about one twentieth the rate of the bar in the $m_K=12$ model, even

though both are pure disc models with no halo component. The instability is therefore of no practical significance since we evolved the model for 40 rotation periods, a time comparable to the believed ages of galaxies, during which no visible feature appeared.

Our results are also consistent with previous studies of the stabilizing effects of halo mass. We find that $q \simeq 0.25$ is the point of marginal bar stability in a disc with very little random motion. However, models in this region of the plane were not featureless, but exhibited multi-arm transient spiral instabilities before forming a bar. Previous experience suggests that even bar-stable models would exhibit three- (or multi-) armed spiral patterns.

6.3 HOT CENTRES ARE ALL THAT IS REQUIRED

Toomre's axisymmetric stability parameter Q (equation 2) combines random motion and the disc-halo ratio. Being a locally defined quantity, its value varies with radius in our models as shown in Fig. 1(c), (f), (i) and (l). In Fig. 3(a) we plot the mass weighted average value of Q over the radius range $r=0$–r_m against growth rate of the *most rapidly growing* bi-symmetric mode measured in these models. Only the two points drawn with dashed symbols lie off a very tight correlation; these two models have small values of q (namely 0.5 and 0.4) and are the only two to possess more rapidly growing $m=3$ modes than the most unstable $m=2$ mode. If all non-axisymmetric modes were considered these two points should be moved upwards: the growth rates of the most rapidly growing disturbances were about 0.3, for the cooler of these two, and 0.25–0.3 for the other.

However, the growth rates of the most unstable bi-symmetric modes correlate very weakly, if at all, with the value of Q far out in the disc. To illustrate this we plot growth rates against Q values at $r=\sqrt{8b}$ in Fig. 3(b). This arbitrarily chosen radius encompasses two thirds of the disc mass; however, any other large radius gives a similar plot. From this we infer that the growth rates of unstable modes are insensitive to the degree of random motion far out in the disc.

6.4 A NON-AXISYMMETRIC STABILITY CRITERION?

The correlation in Fig. 3(a) suggests that $Q \simeq 2.2$ is all that is required to prevent non-axisymmetric instabilities in this mass distribution, irrespective of the fraction of halo.

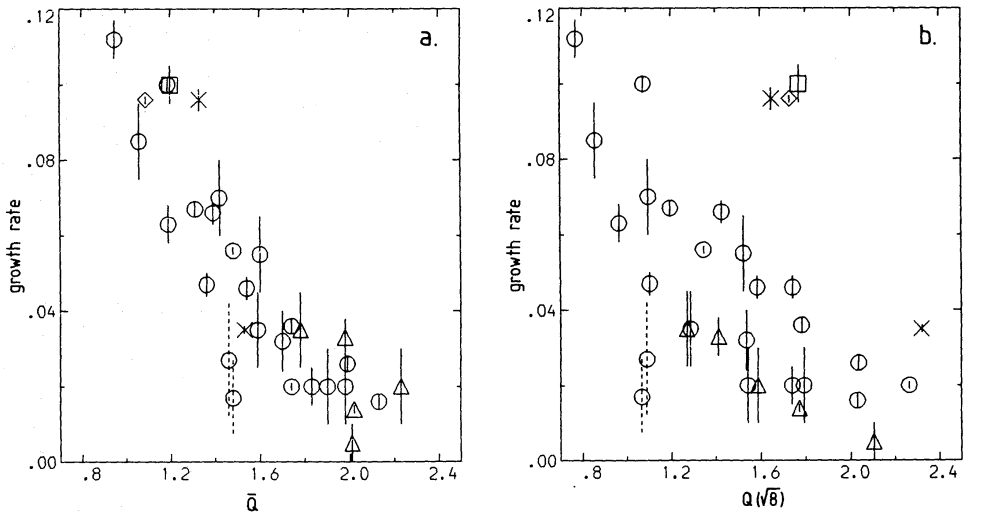

Figure 3. The growth rate of the *fastest growing* bi-symmetric mode in each of the models as functions of (a) the mean Q between the centre and r_m and (b) the value of Q far out in the disc ($r=\sqrt{8b}$). The symbols have the same meaning as in Fig. 2. The two points drawn with dashed error bars are from models having more rapidly growing $m=3$ modes.

Although we omit discussion of them in this paper, we note here that there were no detectable multi-armed instabilities at these high Q values either.

A similar conclusion can be inferred from two other published N-body experiments where reliable Q values are given. Hohl (1971) experimented with cooling his high-Q model and reported that instabilities quickly intervened to reheat the disc whenever he tried to cool it below $Q=2$. Sellwood & Carlberg (1984) found an asymptotic approach to a limiting value of Q in the range 2–2.5 in an uncooled model, independent of softening. In their case, the spiral perturbations responsible for the heating seemed unable to develop at this limiting Q. Both these calculations study mass distributions different from that used here, but indicate very similar limiting Qs. Most other published experiments either do not quote a Q value or are unreliable (e.g. because they use too coarse a spatial grid).

Thus evidence from N-body models seems to indicate that $Q \geqq 2$–2.5 might be a general non-axisymmetric stability criterion. Unfortunately, counter examples are already known from the analytical results of Kalnajs (1972) for uniformly rotating discs and in Zang's (1976) results from self-similar discs. We would, however, like to point out that both these special potentials probably admit a more restricted range of instabilities than those available to a disc with a more general rotation curve.

6.5 COMPOSITE MODELS

Our two experiments with particles chosen in equal proportions from two very different distribution functions do not stand out from the general trends described so far. Their instabilities are simply characterized by the total extent of random motion in the composite stellar distribution.

Both of these models have 50 per cent of their mass in an $m_K=20$ function and the remainder in a much hotter function. It is interesting to compare these to another of our models having the same fraction of mass in the same cool component but with the remaining mass frozen. From Table 1 we see that the growth rate of the bar mode is reduced by almost a factor of 3 as a strongly rotating $m_K=4$ hot component is replaced by a non-rotating $m_K=3$, and that the growth rate is lowered by a further 33 per cent when the non-rotating but active component is replaced by a frozen halo.

Thus the bar mode is able to elicit a strong supporting response from a hot but still rotating population, but a considerably weaker one from the non-rotating population, even when confined to the plane. Were the hot population to have a spheroidal distribution, very few stars would have orbits which remain close to the disc plane and the supporting response would be very small. The resulting growth rate would probably be close to that we observe in the frozen halo model.

7 Mechanism for the modes

Toomre (1981) proposes a mechanism for bar forming modes involving feedback to the swing amplifier via waves passing through the centre. We interpret our results within the framework of this theory.

7.1 NO INNER LINDBLAD RESONANCES

In Fig. 4(b) we plot the growth rates of the *bar* modes against their pattern speeds. The dashed horizontal line in this plot indicates the maximum of $\Omega-\kappa/2$ in our adopted potential – the principal frequencies for nearly circular orbits are shown in Fig. 4(a). The fact that all pattern

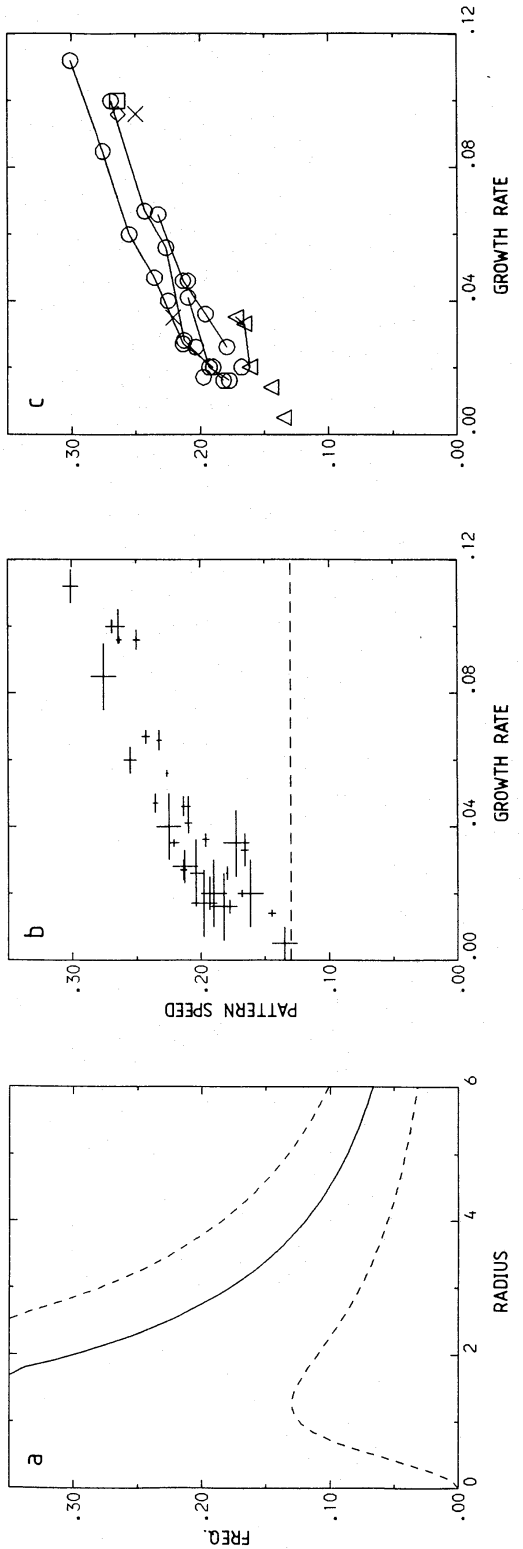

Figure 4. (a) Ω and $\Omega \pm \kappa/2$, for nearly circular orbits in the model potential. (b) A correlation between the pattern speed and growth rate for the *bar* modes. No pattern speed lies below the dashed horizontal line at 0.13, which implies that none of the bar modes has an inner Lindblad resonance. (c). The same data as in (b) but showing the types of distribution function; the symbols have the same meaning as in Fig. 2(b). Points from models having the same velocity distribution but different values of q are joined by lines.

speeds of the bar modes are higher than this implies that none has an inner Lindblad resonance. Thus the main condition for the existence of Toomre's feedback cycle is fulfilled.

7.2 CORRELATION

Fig. 4(b) shows also that higher pattern speeds are associated with higher growth rates. The values given by Kalnajs (1978), Aoki *et al.* (1979) and Toomre (1981) present a similar correlation.

The apparent scatter in the trend is not simply due to noise. Sets of points from models having similar distribution functions but different fractions of active disc lie on similar but systematically displaced curves in this plane, as shown in Fig. 4(c). The symbols joined by lines in this figure come from models employing the same distribution function, but different values of q. The displacement is in the sense that hotter functions have slightly lower pattern speeds for the same growth rate.

7.3 SWING AMPLIFICATION

In Toomre's picture, there are two factors which determine the growth rate: the gain of the amplifier as the wave swings from leading to trailing, and the time required for it to travel to the centre and back to the same point in the cycle. We can use local theory to estimate the amplification factors and travel times (now that we know the pattern speed for each model) and can therefore obtain a local estimate of the growth rate for comparison.

We adopt the simplest local theory to estimate the amplification factor, that designated GLB+LSK in Toomre's (1981) article. We use the shear rate and Q at some appropriate radius for the mode and allow for softened gravity in a straightforward way (see Sellwood & Carlberg 1984). Toomre demonstrates that this crude approximation gives results surprisingly close to those from more careful treatments. The maximum growth factor (MGF) obtainable requires an optimal initial phase for the leading wave. Since all other phases produce less amplification, and could even lead to a reduced amplitude, Toomre (private communication) now favours ½[MGF+1/(MGF)] as a more representative estimate of the actual amplification to be expected. This we denote as net growth factor (NGF).

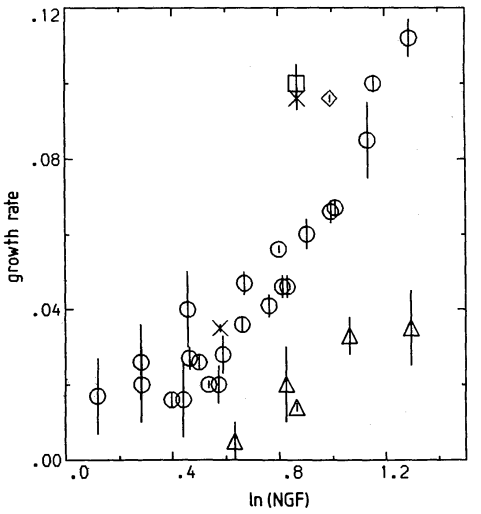

Figure 5. Growth rate of the bar mode as a function of swing amplification factors [ln (NGF)] computed from local theory. The symbols have the same meaning as in Fig. 2(b).

To calculate this quantity, we must choose a radius to determine the relevant shear rate, Q and wavelength. It is clear from Toomre's (1981) fig. 8 that the outgoing wave turns back before reaching co-rotation, and that its amplitude and pitch angle change continuously with radius. No single radius can be identified as the point on the cycle where all the amplification occurs.

Thus any radius we choose has to be a compromise where the NGF is reasonably representative of the amplification round the cycle. After experimenting with several choices, we found that the radius where $m(\Omega-\Omega_p)=-\frac{1}{2}\varkappa$ seemed appropriate.

We plot ln (NGF) against the growth rates of the *bar* mode at this radius in Fig. 5. The Kalnajs functions (circles) lie in the broad band which defines a correlation between these two quantities, which in itself is good evidence that the growth rate is related to swing amplification. All three points above the trend – namely: the Miyamoto model (diamond), one composite model (cross) and our generalized function with a cooler centre (square) – have rising Q profiles, whereas the points which lie below – our new functions with hotter centres (triangles) – have declining Q profiles. Thus we could reasonably attribute these departures from the correlation to our choice of radius, which for these models may be somewhat unrepresentative of the amplification actually occurring around the cycle.

7.4 LOCAL ESTIMATES OF GROWTH RATES

We can estimate the group velocity of the waves over at least part of the cycle from WKBJ theory (Toomre 1969). This involves finding the radius range where solutions to the Lin–Shu–Kalnajs dispersion relation exist in our models at the pattern speed which we measured. No steady WKBJ solutions existed for nine of our models (with gravity softening corrections included), but for the remainder we were able to calculate the WKBJ group velocity and hence make a very rough estimate of the travel time.

Thus, for the majority of our models we can derive a purely local estimate of the growth rate from the ratio ln (NGF)/(travel time), under the additional assumption that our travel times are the complete cycle times. In Fig. 6 we compare these local estimates to our measured values for those models where WKBJ solutions exist. Considering the rough nature of the local treatment, the correlation is surprisingly good, and is strong evidence in favour of Toomre's theory.

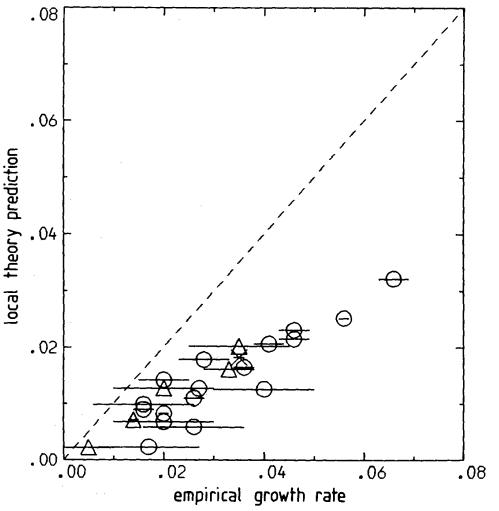

Figure 6. Estimates of growth rates derived from rough local theory compared with our measured values. Local estimates can be made for only 23/32 of our models, but for these they are able to account for about half our observed growth rates. The dashed line has unit slope.

The local estimates are typically about half the actual growth rates; however, a few are closer than this while others are much further away. It is not too surprising that local theory consistently underestimates growth rates, since the amplification factors from global calculations (Toomre 1981, fig. 7) are larger, and since we have also made no allowance for density gradient corrections, which would further increase the amplification.

8 Comparison with observations

Our results can be used to give some indication of the minimum fraction of halo mass required for disc stability when allowance is made for random motion.

Since all our models have the same rotation curve, the marginal stability line of Fig. 2(a) applies only to this one mass distribution. However, we consider that stability requirements would not be very different in other potentials where the rotation curve *rose gently* over a wide range of radii. We would expect our results to apply to low-luminosity galaxies, if any, since Rubin (1983) and her co-workers find that these generally have gently rising rotation curves.

Unfortunately, few measurements of velocity dispersions in disc galaxies are available and hardly any where the rotation curve rises gently. The best case is NGC 7184 reported by van der Kruit & Freeman (1985). Their table 3 and fig. 6 suggest a value for $\sigma_u/\langle v\rangle$ of 165/238=0.69 at the 'turnover radius' i.e. where the rotation curve becomes flat. Reading from our Fig. 2(a), we find that the spheroidal material in this galaxy need provide merely 30 per cent of the central attraction at this radius for the entire system to be stable. This is a considerably smaller fraction than would be required in the absence of the observed pressure support.

Values of $\sigma_u/\langle v\rangle$ at the turnover radius in other galaxies are: 0.6 for NGC 1553 (Kormendy 1984), 2.2 for NGC 1068, 0.6–0.7 for NGC 488 (Kormendy & Illingworth 1985, in preparation) and 0.4–0.6 for NGC 3115 (Illingworth & Schechter 1982) but the rotation curves of these galaxies probably rise too steeply for our stability condition to be applicable.

9 Conclusions

In this paper we have presented a thorough investigation of the role of random motion in controlling bi-symmetric instabilities in one simple mass distribution. Our main results are summarized in Fig. 2(a) which shows that it is possible to reduce the growth rate of the bar instability to a completely insignificant level merely by increasing the random motion amongst the disc stars. It also shows that there is a simple trade-off between the random motion required for stability and the fraction of the radial force arising from a spheroidal bulge/halo material.

Our results are probably relevant to only those galaxies having gently rising rotation curve, and for these we give a simple criterion for the fraction of halo mass required for bar stability in terms of the directly observable ratio $\sigma_u/\langle v\rangle$. The velocity dispersion measurements in the current literature provide only one galaxy for which we can deduce the bulge/halo mass required. In this case taking random motion into account reduces the central attraction required from the bulge/halo from about 70 to 30 per cent of the total force. Thus the observed degree of random motion makes a substantial contribution to stability.

We find that the growth rates of the bar modes correlate strongly with the central value of Q, but scarcely at all with the Q value further out in the disc. Thus we deduce that only hot disc centres are required, and that the outer discs can be cool without making an appreciable difference to the overall bar stability.

Comparison with results from other reported N-body experiments leads us to suggest tentatively $Q\simeq 2$–2.5 at all radii as a sufficient criterion for non-axisymmetric stability in all disc

mass distributions. Where Q is lower than this, bar or spiral instabilities should be present which will ultimately heat the disc until it is stable.

We find good evidence in support of Toomre's (1981) mechanism for bar modes – local theory estimates based on his suggested feedback loop agree with our measurements to the accuracy we could reasonably expect.

Our measurements are confined to one particular family of mass models. Whereas similar results are available for uniformly rotating discs (Kalnajs 1972) and for self-similar discs (Zang 1976), our results are for one instance of more general discs. But it would be dangerous to apply our quantitative results to other mass distributions until it has been demonstrated that a wide variety of models behave in a similar manner.

Acknowledgments

We thank Alar Toomre for helpful comments on the first draft of the paper. The simulations were carried out partly on the Cray 1S at Daresbury under SERC research grant no. SGC/14109, partly on the Cray 1S at Saclay and partly on the 'STARLINK' VAX in Cambridge.

References

Aoki, S., Noguchi, M. & Iye, M., 1979. *Publs astr. Soc. Japan,* **31,** 737.
Athanassoula, E., 1984. *Phys. Repts,* **114,** 319.
Bardeen, J. M., 1975. In: *The Dynamics of Stellar Systems, IAU Symp. No. 69,* p. 297, ed. Hayli, A., Reidel, Dordrecht, Holland.
Combes, F. & Sanders, R. H., 1981. *Astr. Astrophys.,* **96,** 164.
Efstathiou, G., Lake, G. & Negroponte, J., 1982. *Mon. Not. R. astr. Soc.,* **199,** 1069.
Habing, H. J., Olnon, F. M., Winneberg, A., Matthews, H. E. & Baud, B., 1983. *Astr. Astrophys.,* **128,** 230.
Hockney, R. W. & Brownrigg, D. R. K., 1974. *Mon. Not. R. astr. Soc.,* **167,** 351.
Hohl, F., 1971. *Astrophys. J.,* **168,** 343.
Hohl, F., 1978. *Astr. J.,* **83,** 768.
Illingworth, G. & Schechter, P. L., 1982. *Astrophys. J.,* **256,** 481.
James, R. A. & Sellwood, J. A., 1978. *Mon. Not. R. astr. Soc.,* **182,** 331.
Kalnajs, A. J., 1972. *Astrophys. J.,* **175,** 63.
Kalnajs, A. J., 1976. *Astrophys. J.,* **205,** 751.
Kalnajs, A. J., 1977. *Astrophys. J.,* **212,** 637.
Kalnajs, A. J., 1978. In: *Structure and Properties of Nearby Galaxies, IAU Symp. No. 77,* p. 113, eds Berkhuisjen, E. M. & Wielebinski, R., Reidel, Dordrecht, Holland.
Kormendy, J., 1981. In: *The Structure and Evolution of Normal Galaxies,* eds Fall, S. M. & Lynden-Bell, D., Cambridge University Press.
Kormendy, J., 1984. *Astrophys. J.,* **286,** 116.
Miyamoto, M., 1971. *Publs astr. Soc. Japan,* **23,** 21.
Ostriker, J. P. & Peebles, P. J. E., 1973. *Astrophys. J.,* **186,** 467.
Rubin, V. C., 1983. In: *Internal Kinematics and Dynamics of Galaxies, IAU Symp. No. 100,* p. 3, ed. Athanassoula, E., Reidel, Dordrecht, Holland.
Schmidt, M., 1985. In: *The Milky Way Galaxy, IAU Symp. No. 106,* p. 75, eds van Woerden, H., Allen, R. J. & Burton, W. B., Reidel, Dordrecht, Holland.
Sellwood, J. A., 1980. *Astr. Astrophys.,* **89,** 296.
Sellwood, J. A., 1985. *Mon. Not. R. astr. Soc.,* **217,** 127.
Sellwood, J. A. & Athanassoula, E., 1986. *Mon. Not. R. astr. Soc.,* **221,** 195 (Paper 1).
Sellwood, J. A. & Carlberg, R. G., 1984. *Astrophys. J.,* **282,** 61.
Toomre, A., 1963. *Astrophys. J.,* **138,** 385.
Toomre, A., 1964. *Astrophys. J.,* **139,** 1214,
Toomre, A., 1969. *Astrophys. J.,* **158,** 899.
Toomre, A., 1977. *Ann. Rev. Astr. Astrophys.,* **15,** 437.
Toomre, A., 1983. In: *Internal Kinematics and Dynamics of Galaxies, IAU Symp No. 100,* p. 186, ed. Athanassoula, E., Reidel, Dordrecht, Holland.

Toomre, A., 1981. In: *The Structure and Evolution of Normal Galaxies,* eds Fall, S. M. & Lynden-Bell, D., Cambridge University Press.
van der Kruit, P. C. & Freeman, K. C., 1985. *Astrophys. J.*, submitted.
Zang, T. A., 1976. *PhD thesis,* Massachusetts Institute of Technology.

Appendix A

The distribution functions given by Kalnajs (1976) are of the form $e^{m-1}g_m(x)$ where e and x are dimensionless quantities related to the specific energy, E, and specific angular momentum, J, through

$$e=\frac{E}{\phi(0)} \qquad \text{and} \qquad x=-(-2E)^{1/2}\frac{J}{r_*\phi(0)}.$$

Kalnajs also defines the following auxiliary variables

$$w=\frac{\phi}{\phi(0)} \qquad \text{and} \qquad y=\frac{r\phi}{r_*\phi(0)}$$

where ϕ is the gravitational potential and

$$r_*=\lim_{r\to\infty} r\phi/\phi(0).$$

Equilibrium distribution functions can be derived by writing the surface density, Σ, as a function of both w and y. Kalnajs favours the factorization

$$\Sigma(w,y)=w^m\tau(y), \qquad m>0$$

which gives the distribution function noted above. We experimented with a number of alternative factorizations and selected

$$\Sigma(w,y)=w^m\exp(-\beta w^2)\tau'(y)$$

with β an additional free parameter. Following the procedure set out by Kalnajs we find the distribution function to be

$$f(e,x)=\frac{\exp(\beta)}{2\pi^{3/2}}e^{m-1}\sum_{k=0}^{\infty}\frac{(-\beta)^k}{k!}e^{2k}$$
$$\times\sum_{l=0}^{\infty}\left[\sum_{j=0}^{l}\frac{\beta^j}{j!}\binom{3/2-m/2}{l-j}\right]\left(-\frac{1}{4}\right)^l\frac{\Gamma(2k+2l+m+1)}{\Gamma(l+0.5)\Gamma(2k+m+l)}x^{2l}.$$

This double power series in e and x is the most convenient form we have found for computational purposes.

The additional free parameter, β, allows us to generate a wider class of distribution functions than those given by Kalnajs. The range of β is restricted by the requirement that the phase-space density be positive everywhere.

The $m_L=5, \beta=2$ distribution function is illustrated in Fig. A1. The contours in this figure are drawn at levels $\exp(-n^2/8)\times$the peak; the plus sign shows the circular velocity and the outer circle is drawn at the escape velocity. The density of retrograde stars results from our choice of $J_c=0.7$. It is clear from this figure that the velocity distribution is double peaked and, in particular, the position of rest at the centre of the disc is a local minimum.

These rather unnatural properties may be inevitable if only distribution functions separable in e and x are considered. More general functions may prove more satisfactory, but we have not explored this possibility.

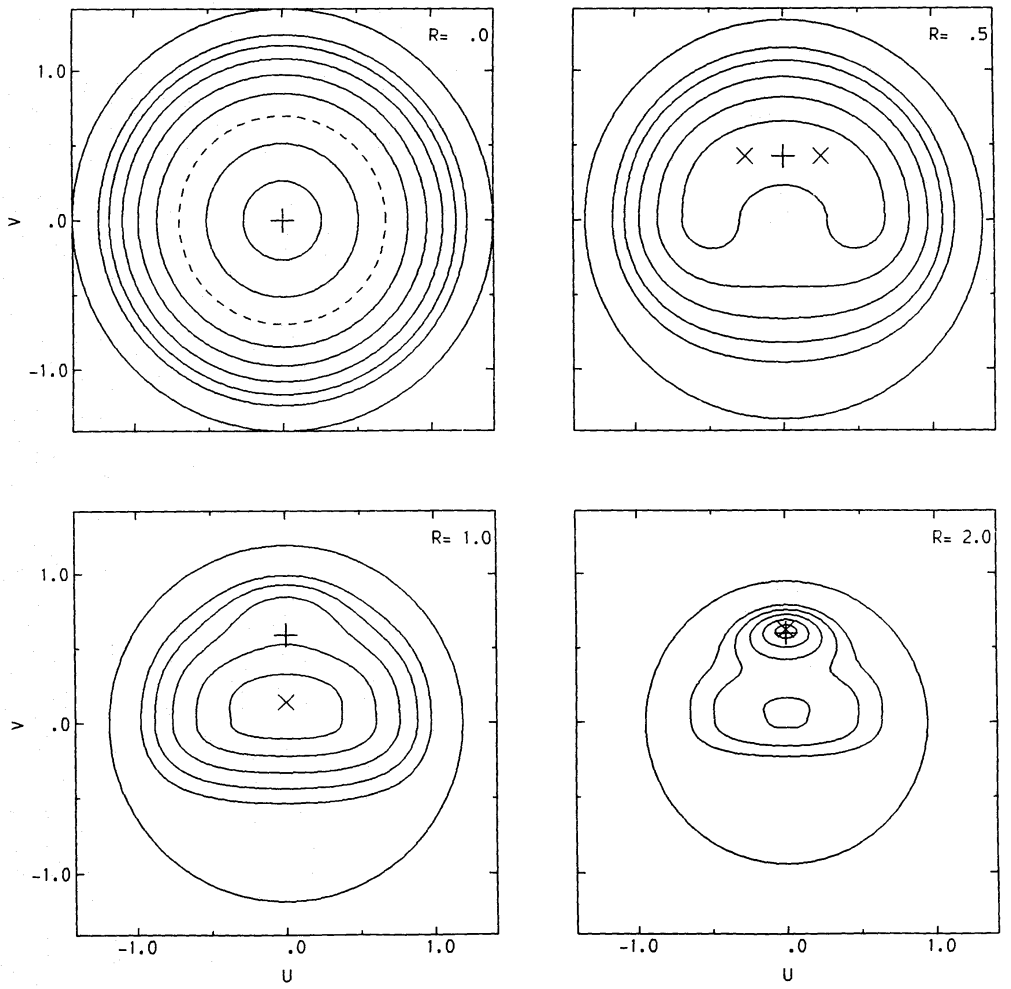

Figure A1. Contours of the $m_L=5$, $\beta=2$ function at four radii. The centre at $r=0$ is a local minimum and the surrounding ridge is marked by a dashed circle. Elsewhere, the function maxima are marked with crosses and the plus sign indicates the circular velocity. The outer circle in each case denotes the escape velocity. The retrograde part is determined according to the rule given in Paper I, with $J_c=0.7$.

Appendix B

Here we describe the behaviour of the additional instability which afflicts only those models started with distribution functions having $\beta>0$.

In addition to the usual rotational instabilities, these models possessed a single, scarcely rotating mode with a very high growth rate. Our estimated eigenfrequency is given in columns 11 and 12 of Table 1 for each of these models. The mode was bi-symmetric, but entirely localized to the region where the distribution function was double peaked, i.e. within about $2b$ of the centre.

Fig. A2 illustrates the typical behaviour of one of these models – that which used the $m_L=8$, $\beta=4$ distribution function. Here we plot contours of over-density at a number of moments during the run. Contour levels are drawn at $(20n-10)$ per cent of the peak value in each plot, recorded in the lower right-hand corner. The two circles are drawn at radii of $0.5b$ and $5b$; data outside this region are excluded since the comparatively low density of particles in those regions gives rise to too much noise.

The rapid growth of this mode ceases very abruptly at about time 100 when its peak relative amplitude is about 20 per cent. This limiting amplitude is so small that the distortion of the particle distribution produced in this or any of the other cases is scarcely visible – it is revealed

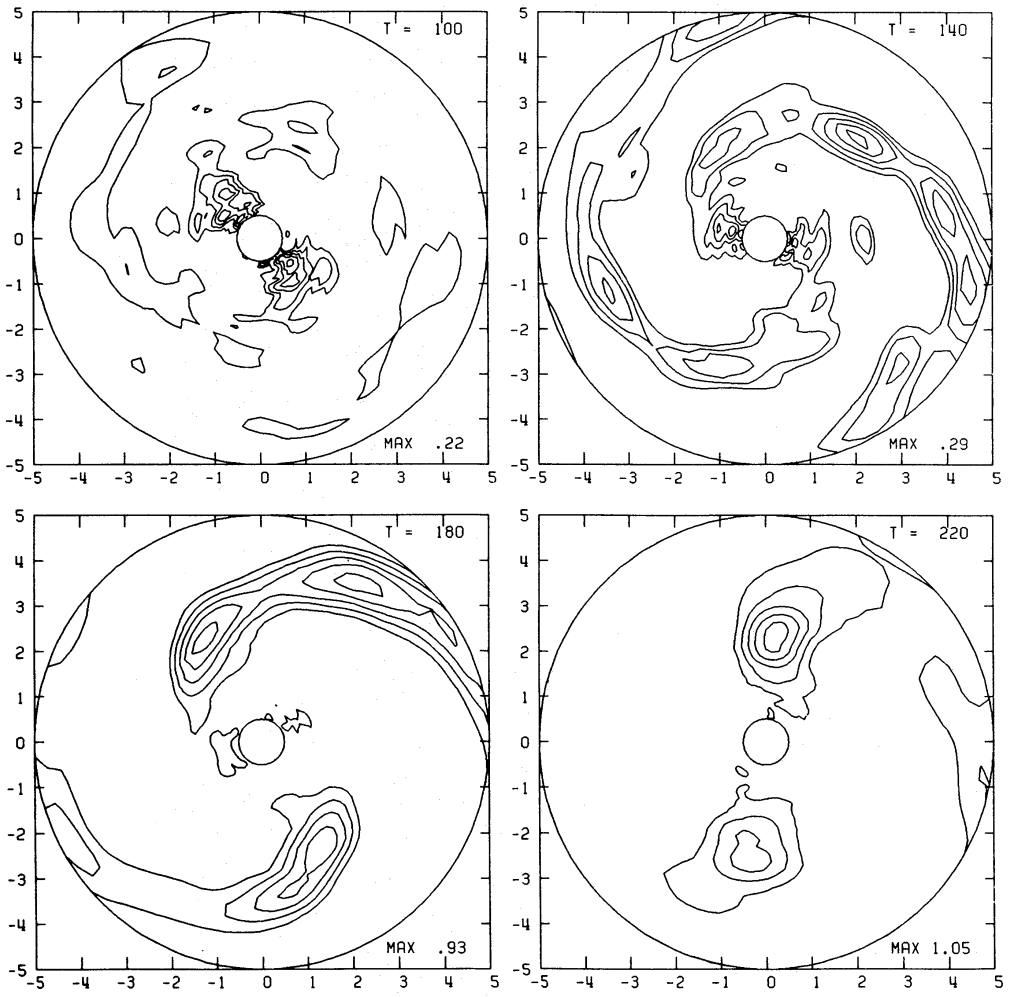

Figure A2. Contours of over-density at four moments in the full-mass disc model which used the $m_L=8$, $\beta=4$ distribution function. The slowly rotating mode reaches its peak amplitude around time 100, after which an orthodox rapidly rotating bar forming mode can be seen. The latter grows more slowly but ultimately dominates the density distribution.

only in such contour plots or through Fourier analysis. The amplitude of this weak bar feature remains nearly constant after time 100, but a more orthodox bi-symmetric mode can be seen, apparently growing linearly, further out in the disc. The second mode has a clear spiral form at times 140 and 180 in Fig. A2, but when it reaches an over-density of order unity, the spirals quickly fade, leaving a strong bar. In all models where we followed the evolution through to completion, the non-linear development of the rapidly rotating second mode is very similar to that of the bar mode in the models with other distribution functions.

Fig. A2 also illustrates how slowly the weak mode rotates and how it is completely decoupled from the bar mode. By the last frame it is visible only in the bottom contour.

It seems evident that this instability arises from the unnatural form of the distribution function, since the velocity distribution is double peaked. One might naïvely expect it to be related to the well-known two-stream instability of plasmas. It is curious that it should be bi-symmetric.